Article

Neuron

Opposing Contributions of GABAergic and Glutamatergic Ventral Pallidal Neurons to Motivational Behaviors

Highlights

- GABAergic and glutamatergic VP neurons oppositely encode motivational value
- They represent internal state and determine behavior during motivational conflict
- GABAergic VP neurons are essential for movements toward reward
- Glutamatergic VP neurons are essential for movements to avoid a threat

Authors

Marcus Stephenson-Jones, Christian Bravo-Rivera, Sandra Ahrens, Alessandro Furlan, Xiong Xiao, Carolina Fernandes-Henriques, Bo Li

Correspondence

bli@cshl.edu

In Brief

Stephenson-Jones et al. show that GABAergic and glutamatergic ventral pallidal neurons control behavior in opposing motivational contexts, by encoding the drive for approaching reward and avoiding punishment, respectively, with the balance between their activities determining approach or avoidance.

Stephenson-Jones et al., 2020, Neuron *105*, 921–933
March 4, 2020
https://doi.org/10.1016/j.neuron.2019.12.006

CellPress

Neuron
Article

Opposing Contributions of GABAergic and Glutamatergic Ventral Pallidal Neurons to Motivational Behaviors

Marcus Stephenson-Jones,[1,2,5] Christian Bravo-Rivera,[1,5] Sandra Ahrens,[1,3] Alessandro Furlan,[1] Xiong Xiao,[1] Carolina Fernandes-Henriques,[1,4] and Bo Li[1,6,*]
[1]Cold Spring Harbor Laboratory, Cold Spring Harbor, NY 11724, USA
[2]Present address: Sainsbury Wellcome Centre for Neural Circuits and Behaviour, London W1T 4JG, UK
[3]Present address: Centre de Neurosciences Psychiatriques, Hôpital de Cery, 1008 Prilly, Lausanne, Switzerland
[4]Present address: Department of Biology, Hunter College & PhD Program in Biology, The Graduate Center of the City University of New York (CUNY), New York, NY 10065, USA
[5]These authors contributed equally
[6]Lead Contact
*Correspondence: bli@cshl.edu
https://doi.org/10.1016/j.neuron.2019.12.006

SUMMARY

The ventral pallidum (VP) is critical for invigorating reward seeking and is also involved in punishment avoidance, but how it contributes to such opposing behavioral actions remains unclear. Here, we show that GABAergic and glutamatergic VP neurons selectively control behavior in opposing motivational contexts. *In vivo* recording combined with optogenetics in mice revealed that these two populations oppositely encode positive and negative motivational value, are differentially modulated by animal's internal state, and determine the behavioral response during motivational conflict. Furthermore, GABAergic VP neurons are essential for movements toward reward in a positive motivational context but suppress movements in an aversive context. In contrast, glutamatergic VP neurons are essential for movements to avoid a threat but suppress movements in an appetitive context. Our results indicate that GABAergic and glutamatergic VP neurons encode the drive for approach and avoidance, respectively, with the balance between their activities determining the type of motivational behavior.

INTRODUCTION

The decision to approach or avoid depends on the situation in the environment and the internal state of the animal. For example, thirst may encourage animals to seek a water source, but a sated animal may not find this goal worth the energy expenditure or risk (Ydenberg and Dill, 1986). Equally, an extremely thirsty animal may approach a water source despite the known risk of predators.

A key region involved in goal-directed motivation is the ventral pallidum (VP). The VP is the major output structure of the ventral basal ganglia (Heimer et al., 1997). It receives projections from areas including the nucleus accumbens (NAc), prefrontal cortex, and basolateral amygdala and transmits information to multiple brain regions involved in motor control and motivation, such as the ventral tegmental area (VTA), lateral habenula (LHb), mediodorsal thalamus, and pedunculopontine tegmental nucleus (Haber and Knutson, 2010). This connectivity places the VP in an ideal location to transform information about the expected value of stimuli into motivation (Mogenson et al., 1980). In particular, the VP sends a major projection to the LHb (Haber and Knutson, 2010; Humphries and Prescott, 2010), a structure that has been shown to regulate both positive and negative reinforcement learning (Lammel et al., 2012; Lecca et al., 2017; Stamatakis et al., 2013; Stamatakis and Stuber, 2012; Stephenson-Jones et al., 2016; Stopper and Floresco, 2014; Tian and Uchida, 2015). Thus, some of the behavioral roles of the VP neurons could be mediated by the VP → LHb pathway.

A large body of work, comprehensively reviewed by others (Humphries and Prescott, 2010; Root et al., 2015; Smith et al., 2009; Stephenson-Jones, 2019), has identified the VP as a crucial driver of reward-seeking behavior. For example, the VP is important for the normal hedonic reactions to sucrose (Farrar et al., 2008), and lesions to the VP decrease an animal's willingness to work for reward (Farrar et al., 2008; Richard et al., 2016). Conversely, rats will work to electrically self-stimulate their VP (Panagis et al., 1995, 1997), and pharmacological activation and disinhibition of the VP can both trigger feeding in sated animals (Stratford et al., 1999).

The VP is also implicated in avoidance behaviors (Stephenson-Jones, 2019; Wulff et al., 2018), as intra-VP mu-opioid activity is sufficient to drive conditioned place aversion (Skoubis and Maidment, 2003), and activating mu opioid receptors in the VP can impair conditioned taste avoidance (Inui and Shimura, 2017). In a similar manner, disinhibiting the VP through injections of the GABAergic antagonist bicuculline induces anxiety-related behaviors and increases avoidance in an approach/avoidance task in primates (Saga et al., 2017; Smith and Berridge, 2005). These findings suggest that the VP plays a role in the motivation to both seek reward and avoid punishment.

While the VP appears critical for motivating behavior in appetitive and aversive contexts, how this structure contributes to these opposing motivational drives remains unclear. One possibility is that separate populations of VP neurons drive opposing motivated behaviors. In line with this idea, *in vivo* recordings in the VP have identified two main types of neurons that are activated by the prediction of either reward or punishment (Richard et al., 2016; Saga et al., 2017; Tachibana and Hikosaka, 2012). These neurons encode information related to the expected or incentive value of stimuli (Richard et al., 2016; Tian et al., 2016; Tindell et al., 2006) and their responses are modulated by the internal state of the animal (Tindell et al., 2006). These different populations of VP neurons may be molecularly distinct, because recent optogenetic activation experiments revealed that activation of GABAergic or glutamatergic VP neurons is reinforcing or aversive, respectively (Faget et al., 2018; Knowland et al., 2017; Tooley et al., 2018).

However, despite these findings, how the GABAergic or glutamatergic VP neurons normally participate in naturalistic and motivational behaviors, and how these neurons are related to the functionally distinct VP neurons observed in *in vivo* recordings, are unknown. Here, our aim was to test the hypothesis that distinct populations of VP neurons play selective roles in appetitive or aversive motivation and determine if GABAergic and glutamatergic VP neurons play opposing roles in the motivation to approach reward or avoid punishment. Our aim was to determine how these populations encode appetitive and aversive motivational value, examine what roles they play in appetitively or aversively motivated behavior, and determine how their interactions influence the overall decision to approach or avoid.

RESULTS

Mapping Functional Classes onto Neurochemical Identities in the VP

In order to determine how GABAergic and glutamatergic VP neurons are engaged by different motivated behaviors, we trained head-fixed mice on a Pavlovian conditioning task. Each trial started with illumination of a house light and proceeded with presentation of an auditory conditioned stimulus (CS) announcing the delivery of one of the following unconditioned stimuli (USs): 0, 1, or 5 μL of water in reward blocks, and 0, 100, or 500 ms of air puff blowing to the face in punishment blocks (Figures 1A and S1A; STAR Methods). As training progressed, mice began licking in response to the reward predicting cues. The lick rate was significantly higher for cues that predicted large rewards than for cues predicting small rewards (Figure S1B) indicating that mice had learnt the CS-US associations.

We recorded the activity of VP neurons (n = 331 neurons/6 mice; 55 ± 15 per mouse) in *Vglut2-Cre;Ai40D* (n = 2) or *Gad2-Cre;Ai40D* (n = 4) mice, in which glutamatergic or GABAergic VP neurons could be optogenetically tagged due to the expression of the light-sensitive proton pump archaerhodopsin (ArchT) (see STAR Methods) (Figures S1C–S1K). Hierarchical clustering revealed that there were four functional classes of VP neurons (Figures 1B and 1C). All identified glutamatergic neurons belonged to one functional cluster (type II). These neurons were activated by punishment-predictive CSs and punishments and inhibited by reward-predictive CSs and rewards; we will refer to these as negative valence neurons (NVNs) (Figures 1B–1D). Two other clusters (types III and IV) contained identified GABAergic neurons (Figures 1B–1D). Type IV neurons were activated by reward-predictive CSs and rewards and inhibited by punishment-predictive CSs and punishments; we will refer to these as positive valence neurons (PVNs) (Figures 1B–1D). As the vast majority of VP neurons are GABAergic (Faget et al., 2018) (and see Figures S1L and S1M), we expected that type IV neurons (PVNs) should outnumber type II neurons (NVNs). Indeed, we recorded a total of 216 PVNs (of which 30 were confirmed to be GABAergic with the tagging) and 34 NVNs (of which 12 were confirmed to be glutamatergic with the tagging). For both the NVNs and PVNs, the magnitude of the CS responses was graded, reflecting the expected magnitude of reward or punishment (Figure 1E). We conclude that these neurons bi-directionally and oppositely encode the positive or negative valences of expected and actual outcomes.

In contrast to these two valence encoding populations, the two other populations appear to encode stimulus saliency as they were excited (type I) or inhibited (type III) by both rewards and punishments or the cues that predict these USs (Figures 1B–1E). Type I neurons were never identified as either glutamatergic or GABAergic and resemble cholinergic basal forebrain neurons that have been described (Hangya et al., 2015). Type III neurons that were inhibited by salient stimuli were identified as GABAergic (Figures 1B–1D).

Over the course of learning, the responses of both PVNs and NVNs to CS increased while their response to positive and negative US decreased, respectively (Figure 2). This reduction in US response in VP neurons is reminiscent of the temporal back-propagation seen in reward prediction error coding dopamine neurons (Cohen et al., 2012; Pan et al., 2005). To examine if these two populations encode reward and punishment prediction errors, we omitted an expected reward in 10% of trials. PVNs displayed a decrease in firing relative to baseline (Figures 3A and 3B), consistent with prediction error encoding. We also analyzed the responses of PVNs to the neutral CS (that predicts nothing) following the house light. As the reward trials and punishment trials were arranged in a block-wise manner in this task, in principle mice should quickly learn if they were likely to receive reward or punishment in a given block. In a reward block, the onset of house light was followed by a reward CS in the majority (~2/3) of trials, but by a neutral CS in a small fraction (~1/3) of trials. As the neutral CS represented the worst situation, it might be perceived as being worse than expected. By contrast, in a punishment block the neutral CS represented the best situation and could be perceived as being better than expected. Consistent with this notion, PVNs displayed a decrease in firing relative to baseline when the neutral cue was presented in a reward block (Figures 3C–3E). In the punishment block, PVNs did not display an increase in firing when the neutral cue was delivered (Figures 3C–3E). This suggests that PVNs selectively respond to reward, but not punishment, prediction errors. NVNs were not significantly modulated when a neutral cue was presented in a punishment block nor were they modulated when the neutral cue was presented in the reward block (Figures 3F and 3G), indicating that these neurons do not

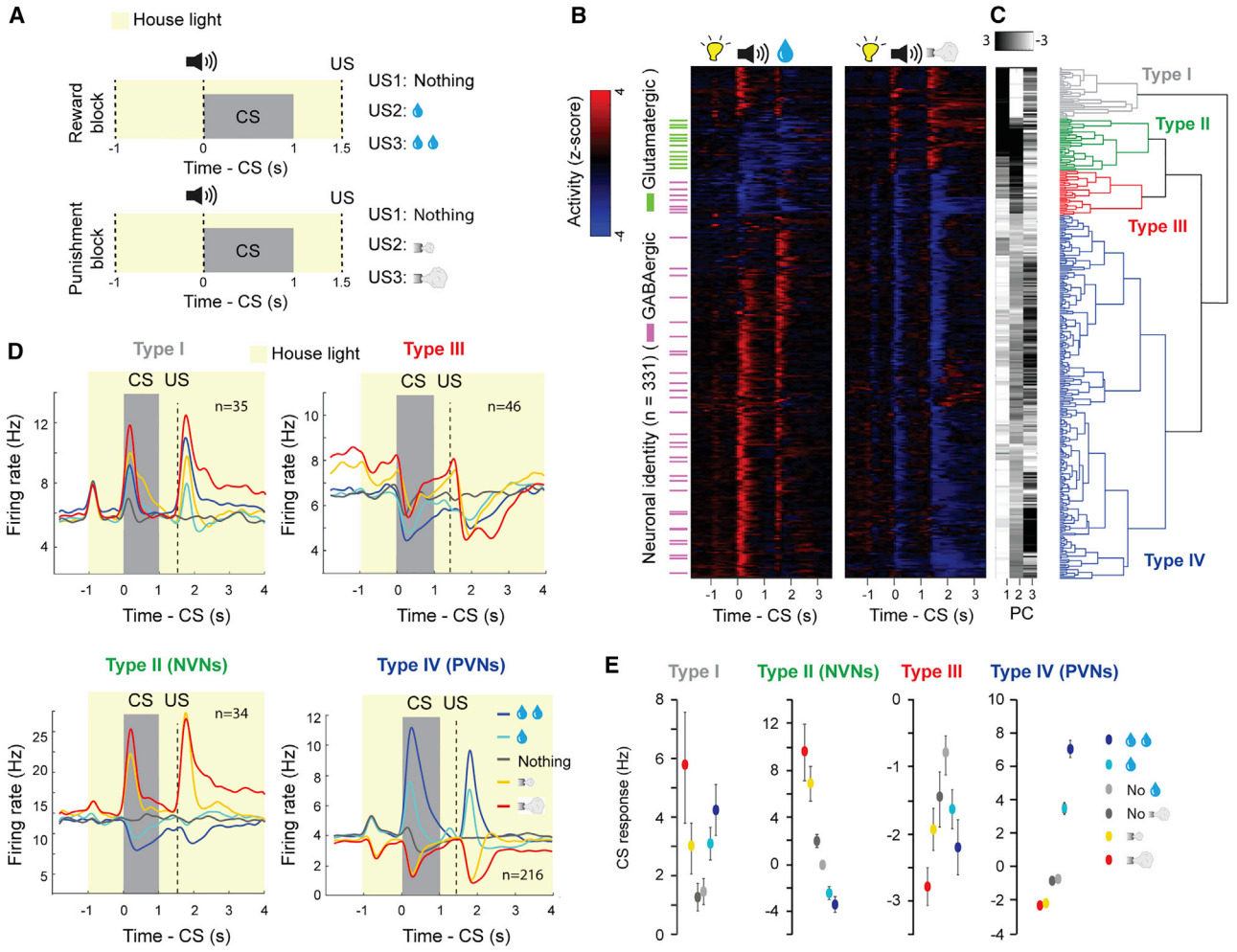

Figure 1. Separate VP Populations Opposingly Encode Motivational Value and Salience

(A) Illustrations of experimental design of the reward and punishment classical conditioning tasks. The neutral CSs are the tones that predict nothing.

(B) *Z* score activity plots of the responses of all neurons recorded in the reward and punishment tasks. Red, increase from baseline; blue, decrease from baseline; each row represents one neuron. Green and purple dashes indicate neurons that were optogenetically tagged as being glutamatergic and GABAergic, respectively.

(C) First three principle components (PC) and hierarchical clustering dendrogram showing the relationship of each neuron within the four clusters.

(D) Average firing rates of the four types of neurons in the reward and punishment blocks, shown as spike density functions (n = 331 from 6 mice).

(E) Average CS response magnitude in the reward and punishment blocks for each of the four types of neurons. All comparisons between the average CS responses were significant (at least $p < 0.05$; Wilcoxon signed-rank test) except between the two neutral CSs (that predict no reward and no punishment in the reward and punishment blocks, respectively, as indicated) in types I, III, and IV neurons. There was also no significant difference between the CS response predicting large and small punishments in type III neurons. Data in (E) are presented as mean ± SEM.

respond when an outcome is better or worse than expected. The properties of the PVNs are similar to those of the reward prediction error-coding dopamine neurons (Cohen et al., 2012; Pan et al., 2005; Schultz et al., 1997).

While prediction error-coding dopamine neurons respond phasically to reward predicting cues, the duration of the CS response in VP PVNs was variable (Figures 3H–3J). Indeed, a number of PVNs had a sustained CS response that lasted till the onset of the US (Figures 3H–3K). Notably, these neurons also appeared to encode prediction error, as in the reward block the activity of these neurons was suppressed by the neutral CS (Figure 3L). The sustained responsive neurons are similar to the VP neurons that have been reported to encode state values (Tachibana and Hikosaka, 2012). However, when sorted for the duration of the CS responses, there did not appear to be two populations of PVNs (phasic and sustained) (Figure 3H), nor did our hierarchical clustering identify two sub-clusters within the population; rather, the population appeared to represent a continuum as has been previously reported (Richard et al., 2016, 2018).

As the VP has been linked to motivation, we examined if the value coding depended on the motivational state of the mice (Figures 4A–4D and S2A–S2D). In the reward sessions of the Pavlovian task, mice showed vigorous licking response starting

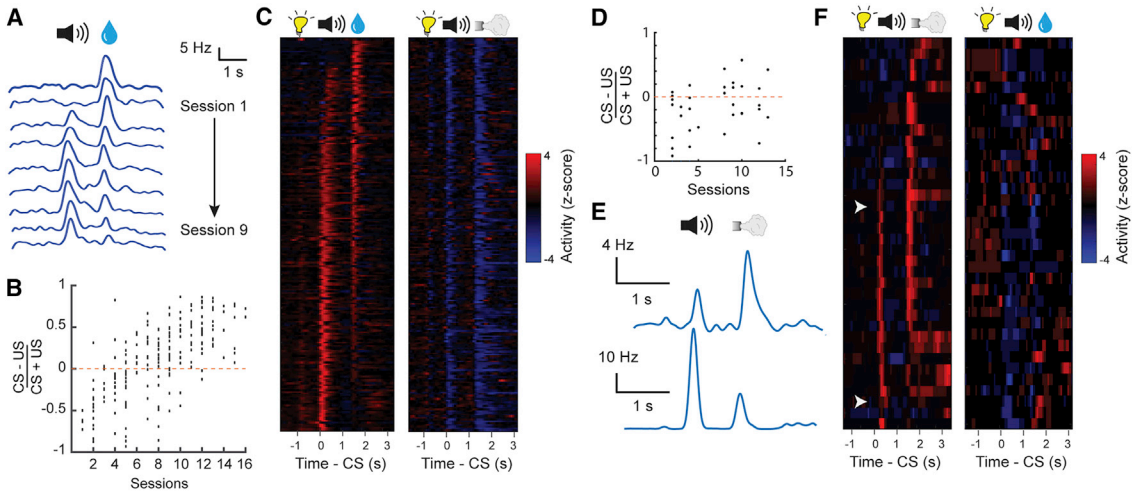

Figure 2. Development of Responses in VP Neurons during Learning

(A) The responses to reward cue (CS) or reward (US) in an example PVN tracked over multiple sessions (S1–S9). Responses are shown as spike density plots.

(B) CS-US (reward) response index for all PVNs across different stages of training (r^2 = 0.69, p < 0.001 by linear regression).

(C) *Z* score activity plots of the responses of all PVNs during reward and punishment blocks. Each row represents the activities of one neuron. Neurons are sorted according to their CS/US response ratio.

(D) The CS/US response index for all NVNs in the punishment block across different stages of training (r^2 = 0.41, p < 0.05 by linear regression).

(E) The CS and US responses of two example NVNs in the punishment block at different stages of training. Responses are shown as spike density plots.

(F) *Z* score activity plots of the responses of all NVNs during reward and punishment blocks. Each row represents the activities of one neuron. Neurons are sorted according to their CS/US response ratio.

from CS onset and lasting until well beyond the delivery of water in the early trials, a period when mice were thirsty, but dramatically reduced licking toward the end of a session (Figures 4B, S2B, and S2D). This decrease in licking presumably reflects a reduction in the motivation to pursue water as the mice were sated. Remarkably, the excitatory CS responses of the PVNs, which were prominent in "thirsty trials," completely disappeared and inverted in "sated trials" (Figures 4A–4D and S2A–S2D). By contrast, the NVNs were differently modulated by animals' thirsty state. While in thirsty trials, these neurons were inhibited by the CS predicting water delivery, in stated trials they were excited by the same CS (Figures 4A and 4D). Notably, thirst also strongly modulated the baseline activities of PVNs and NVNs, such that both populations showed markedly lower baseline activities in sated trials than in thirsty trials (Figures 4C and 4D).

Thus, both changes in the predicted value of the environment and the animal's internal state differentially modulates the activities in PVNs and NVNs, as reflected in both the transient cue-induced responses and the tonic baseline activities in these neurons. These results point to the possibility that PNVs and NVNs differentially and potentially opposingly contribute to the generation of incentive and aversive motivation.

PVNs and NVNs Opposingly and Cooperatively Regulate Motivation

To investigate how PVNs and NVNs might influence the motivation to approach or avoid, we virally expressed channelrhodopsin (ChR2) or ArchT in GABAergic or glutamatergic VP neurons (referred to as PVNs or NVNs, respectively, hereafter for simplicity). We found that optogenetic activation of PVNs or NVNs induced real-time place preference (RTPP) or aversion (RTPA), respectively (Figures S3A–S3D). Furthermore, optogenetic activation of PVNs also supported self-stimulation (Figure S3C). In contrast, optogenetic inhibition of these neurons induced neither RTPP nor RTPA (Figures S3E and S3F). These results, which are largely consistent with previous findings (Faget et al., 2018; Knowland et al., 2017; Tooley et al., 2018), suggest that activation of PVNs or NVNs are innately appetitive or aversive, respectively.

To understand how the PVNs and NVNs contribute to motivated behavior, we first designed a reward-and-punishment conflict task (or "conflict task"), in which incentive value can be modulated by either changing reward size or by introducing punishment (Figure 5A). Specifically, in the reward block of this task, mice needed to lick during a choice window following a CS in order to obtain a water reward, whereas in the conflict block, licking during the choice window led to simultaneous delivery of a water reward and an air-puff in each trial (Figure 5A). In both blocks, different CSs predicted rewards of different sizes. We found that the licking probability during the choice window increased as reward size increased, as would be expected from the associated increase in incentive value. In contrast, the probability decreased when the reward was paired with an air-puff, as would be expected from a decrease in incentive value (Figure 5B).

To test how the different classes of VP neurons influence choice, we optogenetically activated or inhibited these neurons, as described above, during the time window between CS onset and US onset (that covered the choice window) in 20% of randomly selected trials in the conflict task. Notably, activation of PVNs increased the probability that mice would lick in the

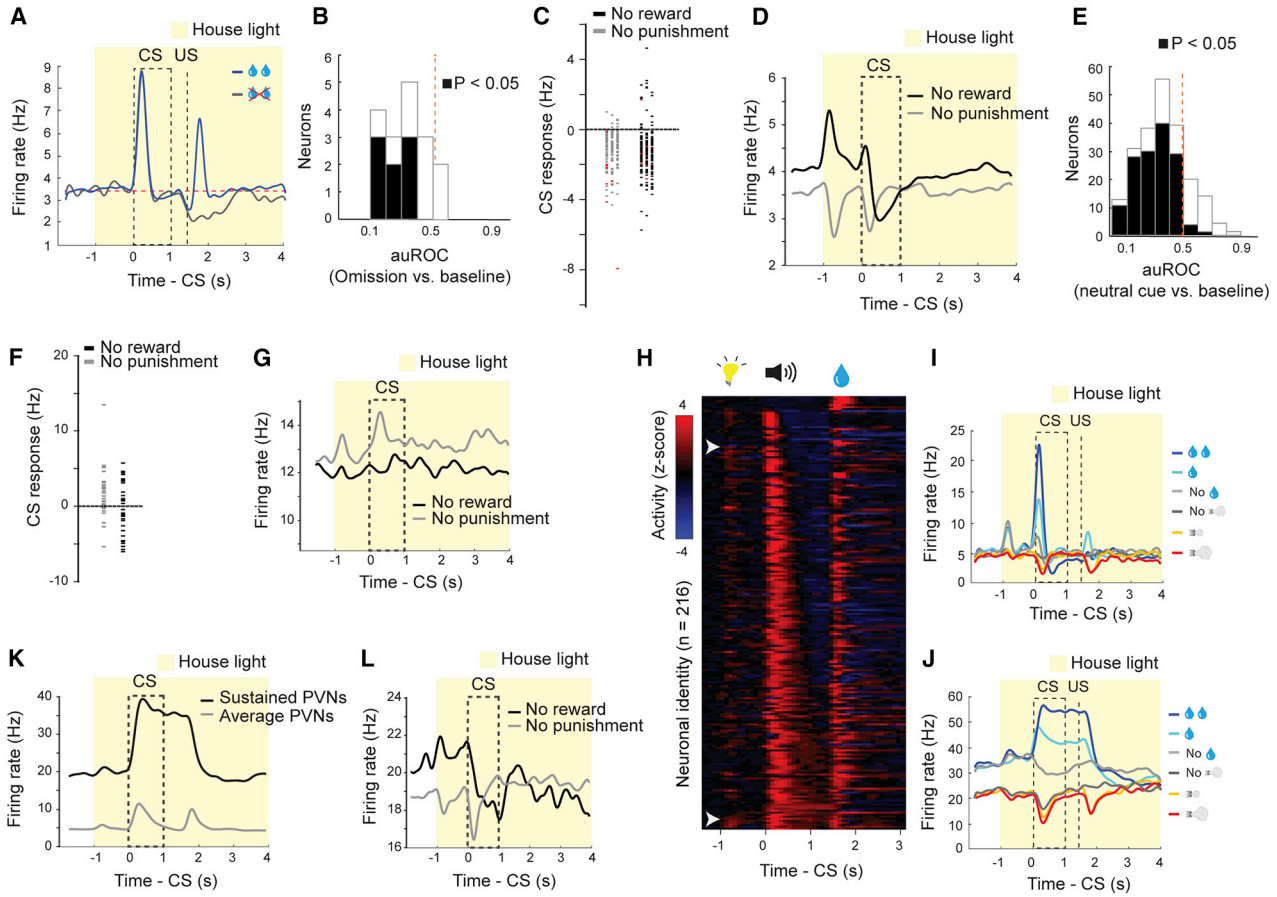

Figure 3. VP Neuron Responses Are Modulated by Expectation

(A) Average firing rates of type IV neurons (PVNs) in response to reward omission, shown as spike density functions.

(B) Area under the receiver operating characteristic (AUROC) analysis of difference in firing rate between baseline and reward omission trials (n = 15 from 2 mice). Filled bars, $p < 0.05$, t test.

(C) Graph showing the CS responses of all PVNs during the neutral cue trials in the reward and punishment blocks (reward block, mean, −1.26 Hz; punishment block, mean, −1.05 Hz). Data points in red come from PVNs with sustained responses to the CS.

(D) Average responses of PVNs during neutral trials in reward and punishments blocks. Responses are shown as spike density plots.

(E) AUROC analysis of difference in firing rate between baseline and neutral cue presentation in PVNs in the reward block (n = 221 from 6 mice). Filled bars, $p < 0.05$, t test.

(F) Graph showing the CS responses of all NVNs during the neutral cue trials in the reward and punishment blocks (reward block, mean, −0.32 Hz; punishment block, mean, −1.96 Hz).

(G) Average responses of NVNs during neutral trials in reward and punishments blocks. Responses are shown as spike density plots.

(H) *Z* score activity plots of the responses of all type IV neurons sorted for the duration of their CS response.

(I and J) Two example neurons showing phasic (I) and sustained (J) responses to reward predicting cues.

(K) Average responses of all PVNs and the PVNs with a sustained response to CS on large reward trials. Responses are shown as spike density plots.

(L) Average responses of the "sustained" PVNs, which showed sustained responses to the CS predicting large reward (see K), to the CS during neutral trials in reward and punishments blocks. Responses are shown as spike density plots.

choice window, in particular when the CS predicted a small reward (i.e., when the motivation to lick was low) (Figure 5C); inhibition of these neurons decreased the probability that mice would lick on a given trial, even if the CS predicted a large reward (i.e., when the incentive to lick was high) (Figure 5D). By contrast, activation of NVNs decreased the probability that mice would lick on a given trial (Figure 5C). Although inhibition of NVNs had no effect on the behavior in reward blocks (Figure 5D), inhibition of these neurons in the conflict blocks increased the probability that mice would lick in a trial (Figure 5E). Importantly, inhibition or activation of PVNs did not influence licking per se, either in thirsty or sated mice (Figures S3G and S3H), indicating that these neurons do not directly control movements. In addition, in control experiments (Figures S4A–S4H) we verified that light illumination alone in the VP had no effect on animal behavior in the conflict task (Figures S4A and S4B). These results suggest that PVNs play an essential role in generating or regulating incentive value. By contrast, NVNs are less critical for reward seeking but are essential for constraining reward seeking when there is a potential adverse outcome associated with the action.

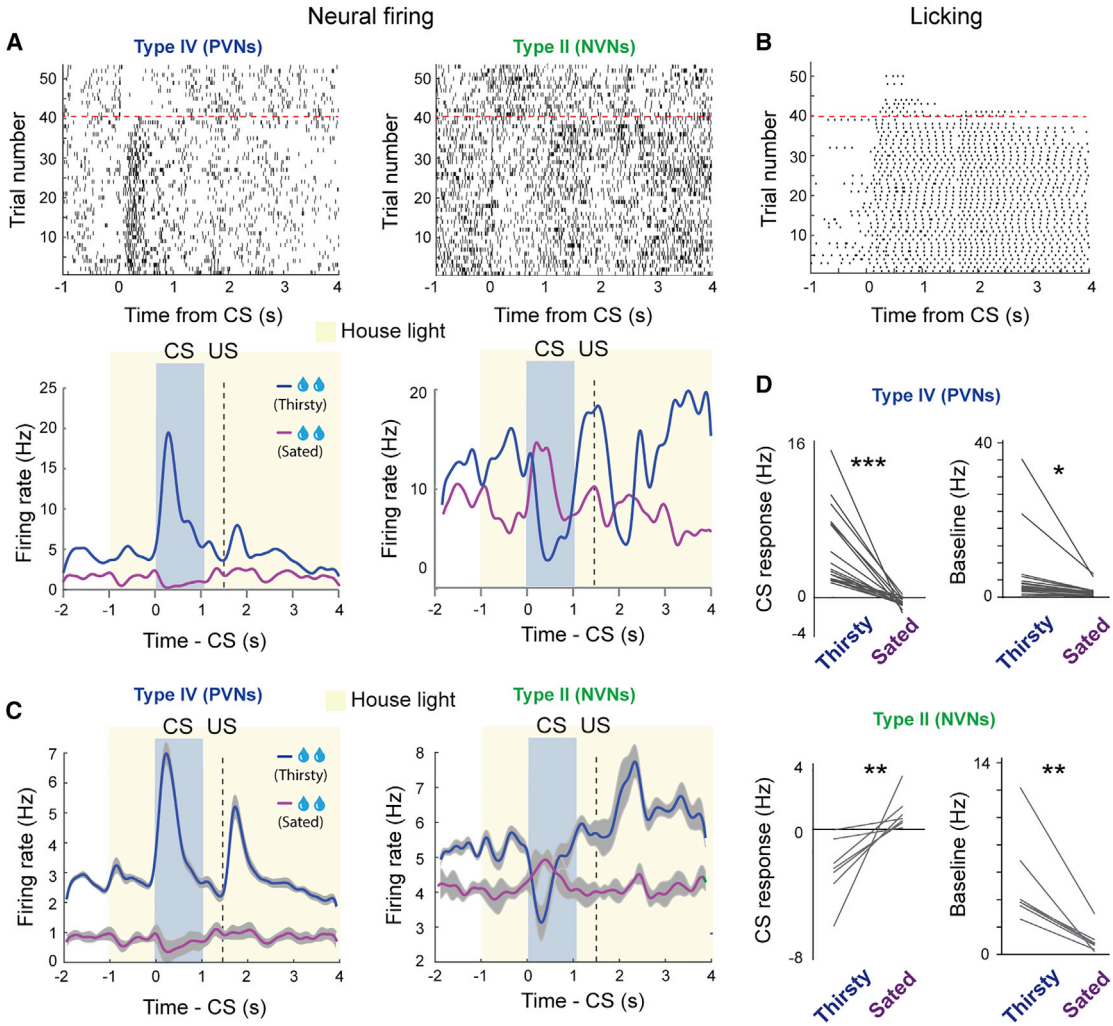

Figure 4. The Response of VP Neurons to Reward Predicting CS Depends on the Internal Motivational State

(A) Top: raster plots showing the neural activity of a PVN (left) and a NVN (right) during large reward trials. Bottom: spike density plots showing the average response of the corresponding two neurons when the mouse was thirsty or sated.

(B) Raster plot showing the licking behavior in the same behavioral session.

(C) Average spike density plots showing the activity of PVNs (n = 19, from 2 mice) and NVNs (n = 7, from 2 mice) in thirsty and sated trials.

(D) Left: graphs showing the average CS response of PVNs (top) and NVNs (bottom) when mice were thirsty or sated. Right: graphs showing the baseline firing rates of PVNs (top) and NVNs (bottom) when mice were thirsty or sated (***$p < 0.001$, **$p < 0.01$, *$p < 0.05$; paired t test). Data in (C) are presented as mean ± SEM (shaded areas).

To determine how the endogenous activities of these VP neurons might be modulated by the "conflict," we recorded VP neurons in mice performing a modified version of the conflict task (see STAR Methods). We found that, in the conflict trials as compared to the reward-only trials, the excitatory CS responses of PVNs were reduced, whereas the activity of the NVNs was higher in the conflict trials (Figures 5F and 5G). These results indicate that perceived risk associated with licking in the conflict task suppresses and increases (or disinhibits), respectively, the responses of PVNs and NVNs to reward cues. These results, together with those from optogenetic manipulations, suggest that the balance between PVN's and NVN's activity sets the motivation to seek the reward when there is a motivational conflict.

While the NVNs do not play a direct role in driving reward-seeking behavior, we hypothesized that they may drive behavior in an aversive context. To determine how PVNs and NVNs contribute to behavior in an appetitive or aversive context, we designed a "run-for-water" (RFW) task and a "run-to-avoid-air-puff" (RTAA) task, respectively (Figures 6A and 6B). In the RFW task, mice needed to run in response to a CS in order to obtain a water reward, whereas in the RTAA task mice had to run in response to a CS in order to avoid an air-puff (Figures 6C and 6D). Once mice learned the tasks, we optogenetically activated or inhibited PVNs or NVNs, as described above, during the time window between CS onset and US onset in 20% of randomly selected trials (Figures 6E–6J and S5). We found

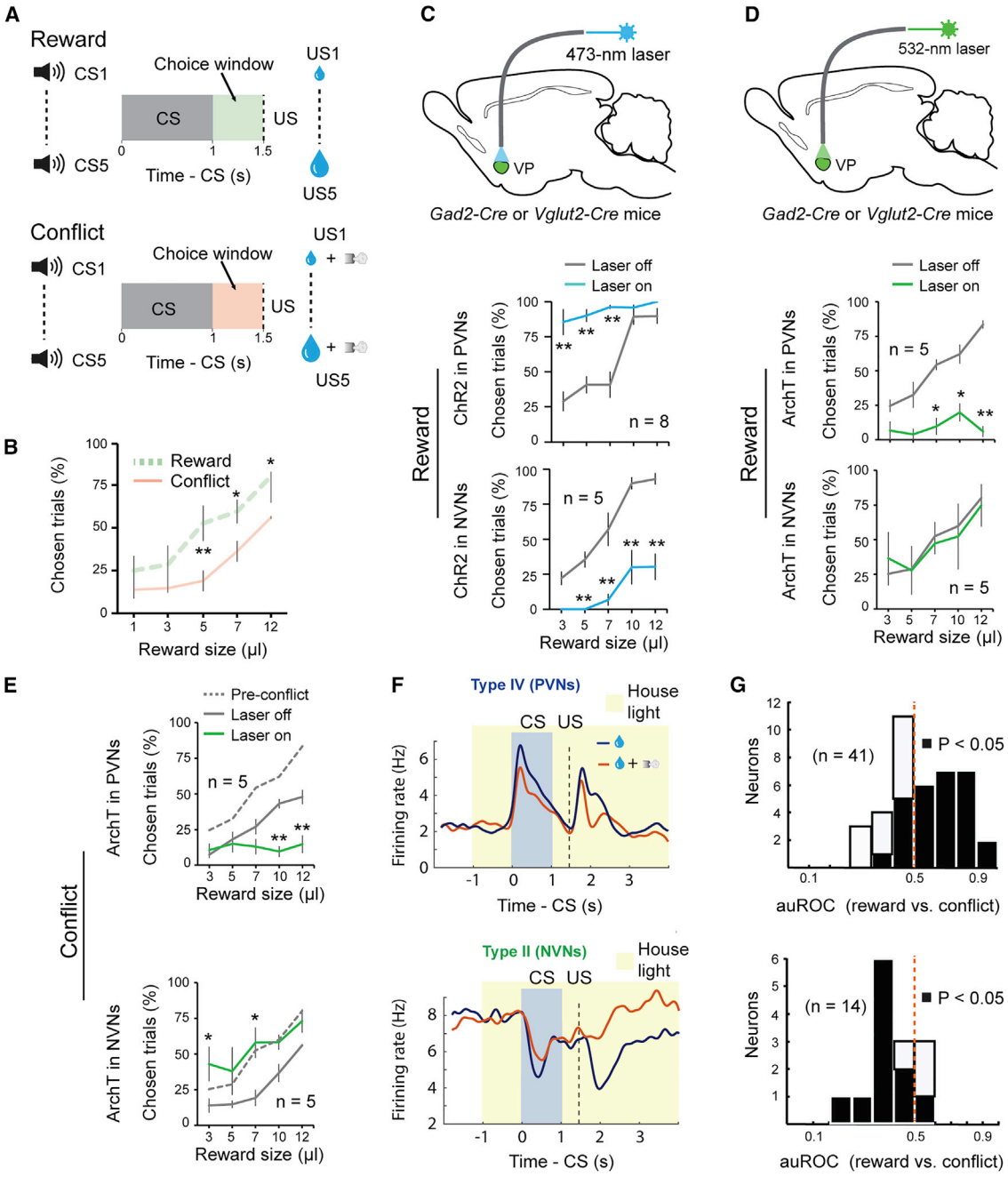

Figure 5. The Balance of Activity between PVNs and NVNs Controls Reward Seeking during Motivational Conflict

(A) Schematics of the experimental design.

(B) Motivational conflict reduced reward seeking ($F_{(1,9)} = 35.19$, $p < 0.0001$). **$p < 0.01$, *$p < 0.05$, two-way ANOVA followed by Tukey's test.

(C) Top: a schematic of the approach. Middle: activation of PVNs increased reward seeking ($F_{(1,15)} = 92.32$, $p < 0.001$). Bottom: activation of NVNs decreased reward seeking ($F_{(1,7)} = 108.68$, $p < 0.001$). **$p < 0.01$, two-way ANOVA followed by Tukey's test.

(D) Top: a schematic of the approach. Middle: inhibition of PVNs decreased reward seeking ($F_{(1,9)} = 50.37$, $p < 0.0001$). Bottom: inhibition of NVNs had no effect on reward seeking ($F_{(1,9)} = 0.055$, $p = 0.82$). **$p < 0.01$, *$p < 0.05$, two-way ANOVA followed by Tukey's test.

(E) Top: inhibition of PVNs further decreased reward seeking in the conflict task ($F_{(1,9)} = 27.60$, $p < 0.0001$). Bottom: inhibition of NVNs increased reward seeking to pre-conflict levels ($F_{(1,9)} = 50.37$, $p < 0.0001$). **$p < 0.01$, *$p < 0.05$, two-way ANOVA followed by Tukey's test.

(F) Average response of PVNs (top; n = 41, from two mice) or NVNs (bottom; n = 14, from two mice) in reward or conflict trials, shown as spike density plots.

(G) AUROC analysis of difference in the CS response during reward and conflict trials. Top: PVNs (n = 41 from two mice); bottom: NVNs (n = 14, from two mice). Filled bars, $p < 0.05$, t test. Data are presented as mean ± SEM.

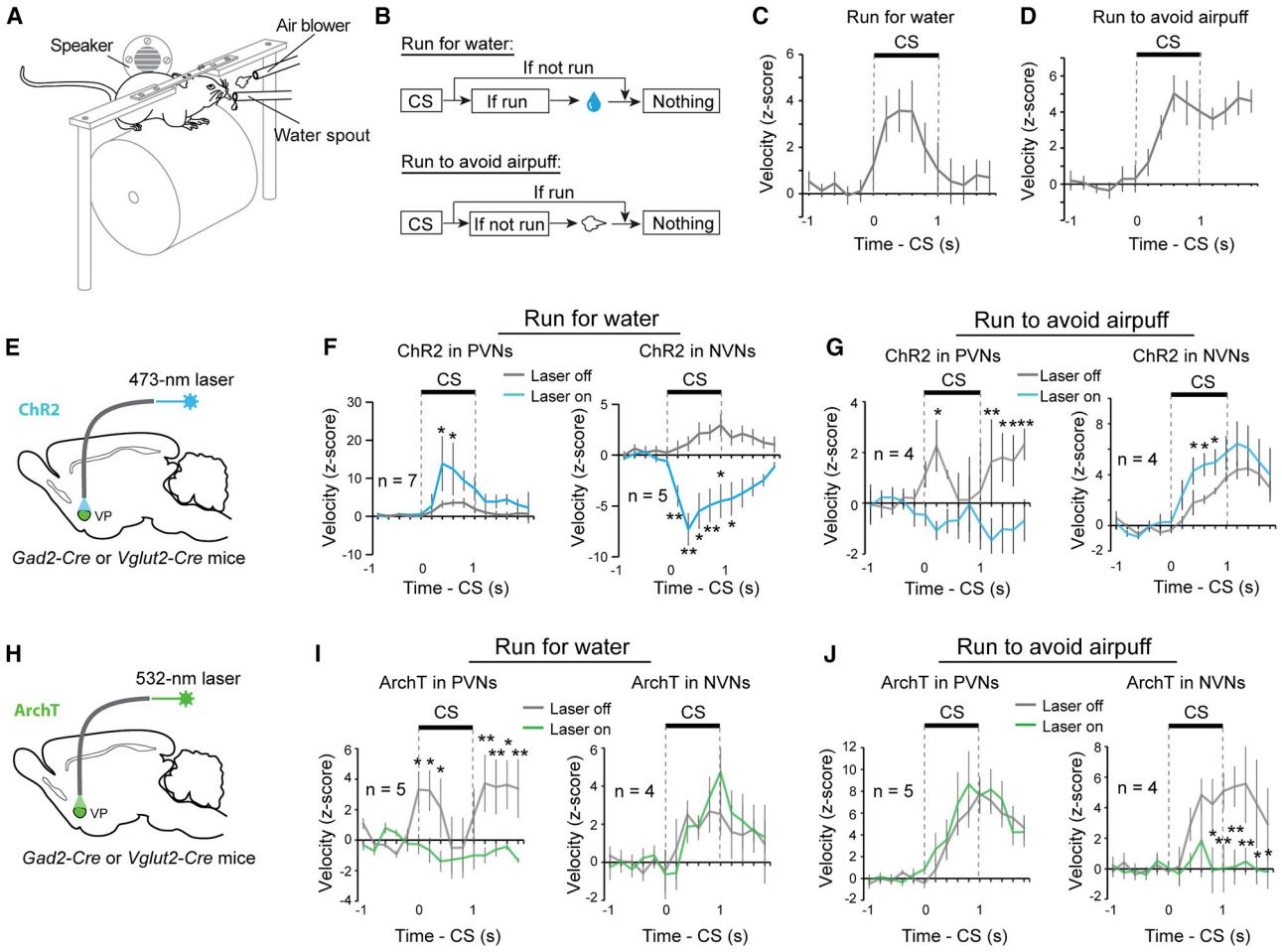

Figure 6. PVNs and NVNs Switch Roles in Controlling Actions When Motivational Context Changes

(A–D) The running tasks. (A) A schematic of the experimental design. (B) Schematics of the experimental procedure. (C) Behavioral performance of mice in the run-for-water task (n = 7). (D) Behavioral performance of mice in the run-to-avoid-air-puff task (n = 4).

(E) Schematics of the approach.

(F) Left: activation of PVNs increased running for water reward ($F_{(1,13)} = 7.90$, $p = 0.0055$). Right: activation of NVNs decreased running for water reward ($F_{(1,9)} = 132.73$, $p < 0.001$). **$p < 0.01$, *$p < 0.05$, two-way ANOVA followed by Tukey's test.

(G) Left: activation of PVNs decreased running to avoid air puff ($F_{(1,7)} = 18.76$, $p < 0.0001$). Right: activation of NVNs increased running to avoid air puff ($F_{(1,7)} = 11.61$, $p = 0.0010$). **$p < 0.01$, *$p < 0.05$, two-way ANOVA followed by Tukey's test.

(H) Schematics of the approach.

(I) Left: inhibition of PVNs decreased running for water reward ($F_{(1,9)} = 29.283$, $p < 0.0001$). Right: inhibition of NVNs had no effect on running for water reward ($F_{(1,7)} = 0.30$, $p = 0.59$). **$p < 0.01$, *$p < 0.05$, two-way ANOVA followed by Tukey's test.

(J) Left: inhibition of PVNs had no effect on running to avoid air puff ($F_{(1,9)} = 1.30$, $p = 0.26$). Right: inhibition of PVNs decreased running to avoid air puff ($F_{(1,7)} = 22.06$, $p < 0.001$). **$p < 0.01$, *$p < 0.05$, two-way ANOVA followed by Tukey's test. Data are presented as mean ± SEM.

that, in the RFW task, activating and inhibiting PVNs promoted and abolished running, respectively (Figures 6E, 6F, 6H, 6I, S4C, and S4D). In contrast, activating NVNs decreased the velocity in the RFW task, while inhibiting these neurons did not affect running (Figures 6E, 6F, 6H, 6I, S4C, and S4D). In stark contrast to the RFW task, in the RTAA task, activating PVNs completely abolished running responses, whereas inhibiting these neurons had no effect (Figures 6E, 6G, 6H, 6J, S4C, and S4D); moreover, activating and inhibiting NVNs promoted and abolished running, respectively (Figures 6E, 6G, 6H, 6J, S4C, and S4D). Thus, while PVNs promote running in a reward-seeking task, activating them suppresses running in a punishment-avoidance task. In the opposite manner, NVNs are essential for promoting running to avoid punishment, but suppress the same behavior when it is being performed to obtain a reward. Of note, males and females behaved similarly in these tasks (Figure S6; Table S1). These results suggest that the motivational context switches the role that each population plays in behavior; in a reward-seeking context PVNs drive the behavior while NVNs constrain the behavior. In an aversive context these roles reverse, with the NVNs driving avoidance behavior and the PVNs actively constraining the avoidance.

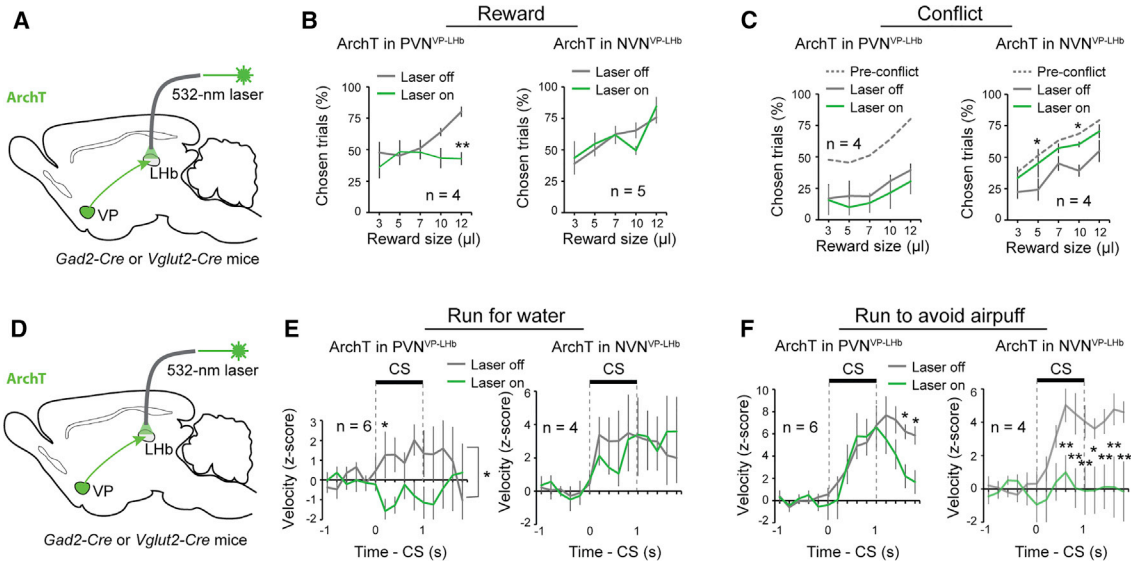

Figure 7. PVNs and NVNs Act via the VP-LHb Pathway

(A) A schematic of the approach.

(B) Left: inhibition of $PVN^{VP \rightarrow LHb}$ decreased reward seeking ($F_{(1,7)} = 9.55$, $p = 0.0043$). Right: inhibition of $NVN^{VP \rightarrow LHb}$ had no effect on reward seeking ($F_{(1,9)} = 0.0041$, $p = 0.95$). $^{**}p < 0.01$, two-way ANOVA followed by Tukey's test.

(C) Left: inhibition of $PVN^{VP \rightarrow LHb}$ did not further decrease reward seeking in these mice in the conflict task ($F_{(1,7)} = 1.39$, $p = 0.25$). Right: inhibition of $NVN^{VP \rightarrow LHb}$ increased reward seeking to pre-conflict levels ($F_{(1,7)} = 13.17$, $p = 0.0010$). $^{**}p < 0.01$, $^{*}p < 0.05$, two-way ANOVA followed by Tukey's test.

(D) A schematic of the approach.

(E) Left: inhibition of $PVN^{VP \rightarrow LHb}$ decreased running for water reward ($F_{(1,11)} = 8.56$, $p = 0.004$). Right: inhibition of $NVN^{VP \rightarrow LHb}$ had no effect on running for water reward ($F_{(1,7)} = 0.060$, $p = 0.81$). $^{*}p < 0.05$, two-way ANOVA followed by Tukey's test.

(F) Left: inhibition of $PVN^{VP \rightarrow LHb}$ had no effect on running to avoid air puff during the cue, although it induced an earlier termination of the running response after the cue ($F_{(1,11)} = 5.57$, $p = 0.020$). Right: inhibition of $NVN^{VP \rightarrow LHb}$ decreased running to avoid air puff ($F_{(1,9)} = 40.72$, $p < 0.0001$). $^{**}p < 0.01$, $^{*}p < 0.05$, two-way ANOVA followed by Tukey's test. Data are presented as mean ± SEM.

PVNs and NVNs Act via the VP–LHb Pathway

In order to explore how downstream structures integrate the activity of PVNs and NVNs, we first looked at the projections of these neurons. Consistent with previous findings, both PVNs and NVNs receive input from areas such as the nucleus accumbens, prefrontal cortex, and basolateral amygdala (Figures S7A–S7G) and project to qualitatively the same structures, including the ventral tegmental area, lateral hypothalamus, lateral habenula (LHb) and rostromedial tegmental nucleus (Root et al., 2015; Tooley et al., 2018). Each of the two functionally distinct populations of VP neurons may synapse onto different cell types within these areas or individual neurons may receive opposing inputs from both of these populations. To explore this, we choose one projection target, the LHb. The VP projects to the medial portion of the LHb (Figure S8) (Herkenham and Nauta, 1977; Root et al., 2015), which in turn projects to the dorsal raphe (DR) (Herkenham and Nauta, 1979; Quina et al., 2015). The DR also has neurons that encode the motivational value (Cohen et al., 2015) and the behavioral effects of serotonin, like those reported here, also depend on the state of the environment (Seo et al., 2019). Retrograde tracing combined with single molecule *in situ* hybridization confirmed that both PVNs and NVNs project to the LHb (Figures S9A–S9C). In addition, using optogenetics combined with electrophysiology in acute slices, we recorded from LHb neurons that were retrogradely labeled from the DR. Every neuron that was recorded received PVN (GABAergic) or NVN (glutamatergic) input, suggesting that individual DR-projecting LHb neurons receive inputs from both VP populations (Figures S9D–S9G).

To determine the behavioral effect of the VP → LHb pathway, we optogenetically activated PVN or NVN axon terminals in the LHb. Activation of the PVN ($PVN^{VP \rightarrow LHb}$) or NVN ($NVN^{VP \rightarrow LHb}$) inputs to the LHb induced RTPP or RTPA, respectively (Figures S8, S10A, and S10B). These results confirmed that both PVNs and NVNs send substantial projections to the LHb that can differentially influence animal behavior, consistent with previous findings (Faget et al., 2018; Knowland et al., 2017; Tooley et al., 2018).

Next, we assessed the roles of $PVN^{VP \rightarrow LHb}$ and $NVN^{VP \rightarrow LHb}$ in the behaviors driven by incentive or aversive value, as described above. In the reward and conflict tasks, we found that optogenetically inhibiting $PVN^{VP \rightarrow LHb}$ decreased choice in the reward-only block (Figures 7A and 7B). This manipulation did not reduce choice in the conflict block, likely due to a "floor effect" as this group of mice were highly sensitive to the punishment (Figure 7C). By contrast, inhibiting $NVN^{VP \rightarrow LHb}$ did not affect choice in the reward-only block, but increased the probability of choice in the conflict block (Figures 7B and 7C).

In the RFW and RTAA tasks (see Figure 6), inhibiting $PVN^{VP \rightarrow LHb}$ abolished running for water (Figures 7D and 7E), but only slightly reduced running to avoid air-puff (Figure 7F). By contrast, inhibiting $NVN^{VP \rightarrow LHb}$ did not affect

running for water (Figure 7E), but abolished running to avoid air-puff (Figure 7F). Of note, inhibition of either pathway did not induce any obvious effects in the RTPP or RTPA task (Figures S10C and S10D). Furthermore, control experiments demonstrated that the behavioral effects we observed were not induced by light illumination per se (Figures S4E–S4H). Together, these results are consistent with the optogenetic manipulations of cells in the VP (Figures 5 and 6), and suggest that the distinct behavioral roles of the GABAergic and glutamatergic VP neurons are, at least in part, mediated by their projections to the LHb.

DISCUSSION

The decision to approach or avoid depends on the situation in the environment and the internal state of the animal. Here, we show that separate populations of VP neurons drive behavior in different motivational contexts, and their activity is differentially regulated by both the valence of the environment and the internal state of the animal. The PVNs are necessary for driving reward-seeking behavior in positive motivational context, while the NVNs are needed for driving avoidance behavior in an aversive motivational context. Previous work had described two types of VP neurons that represent the prediction of either reward or punishment (Richard et al., 2016; Saga et al., 2017; Tachibana and Hikosaka, 2012) and had shown that the VP is important for reward seeking and punishment avoidance (Root et al., 2015; Smith et al., 2009; Stephenson-Jones, 2019; Wulff et al., 2018). However, the identity of the VP cells representing either reward or punishment prediction was unknown. It was also unclear if these distinct VP representations are causally related to valence-specific behaviors and, if so, how they contribute to behaviors in naturalistic settings.

We have now linked the NVNs and PVNs in the VP to glutamatergic and GABAergic neurons, respectively, in *in vivo* recording. To our knowledge, this is the first time that the different functional classes of VP neurons have been mapped onto distinct neurochemical identities. Furthermore, we have designed novel behavioral tasks to probe the precise functions of VP neurons. Previous studies showed that activation of glutamatergic or GABAergic VP neurons induces aversive or preference responses, respectively. Our behavioral tasks, which were designed to mimic naturalistic behaviors, allow us to demonstrate how in normal reward-seeking or punishment-avoidance behavior, or in different behavioral contexts (rewarding versus punishing), the different classes of VP neurons make unique contributions to distinct, adaptive behavioral actions. In particular, we uncover how these two populations interact in risk/reward decision making, and identify a mechanism where the activity of these populations interact in a push/pull manner to determine the overall behavioral strategy. Finally, we show for the first time that the contributions of these distinct VP populations to behavior is state dependent.

In the natural world, reward seeking is associated with certain costs, such as the effort needed to obtain a reward, the risk of punishment or the presence of threats (Ydenberg and Dill, 1986). Our results show that NVNs are needed to constrain reward seeking when there is a risk associated with seeking reward. In line with this, a recent study showed that glutamatergic VP neurons are needed to constrain reward seeking when effort is required to obtain a reward or to limit reward seeking when the reward has been devalued (Tooley et al., 2018). In light of this finding, our results suggest that glutamatergic NVNs represent the risk of punishment associated with seeking-reward and work to balance the incentive value represented by the GABAergic PVNs. In the opposing manner, the internal state of an animal, such as thirst, may encourage animals to take a risk and reduce the likelihood an animal would avoid a threatening environment. Our results now suggest that PVNs can constrain avoidance. Together, our results suggest that the balance between PVN and NVN activity sets the motivation for approach and avoidance.

If the balance between these populations sets the behavioral response in different motivational contexts, how then do downstream neurons read out this balance? Our results suggest one mechanisms by which this is achieved (i.e., individual neurons downstream of the VP receive input from both PVNs and NVNs). In this way, individual neurons can integrate the excitatory and inhibitory input from the VP, with the balance between these drives determining the activity of the postsynaptic neuron. While other patterns of integration likely exist, individual neurons in the VTA also appear to integrate the excitatory and inhibitory input from the VP, as more than half of VTA neurons receive direct GABAergic or glutamatergic VP input (Faget et al., 2018). This suggests that as predicted from their common projection pattern (Faget et al., 2018), the different VP populations have an opposing influence on common downstream targets.

If downstream neurons integrate input from the different VP populations, they should be activated or inhibited in opposing motivational contexts. In line with this, a recent study has shown that GABAergic and serotonergic neurons in the dorsal raphe are selectively activated and drive movement in high threat environments but are inhibited and suppress movement in a rewarding environment (Seo et al., 2019). Interestingly, the VP innervates the medial portion of the LHb that projects to the dorsal raphe (Herkenham and Nauta, 1977, 1979). As with neurons in the VP, the firing rate of the serotonergic neurons is modulated on a short and long timescale by the predicted value and utility of a stimulus (Cohen et al., 2015). This suggests the contextual dependence of raphe activation may be driven by a switch in the balance between PVN and NVN activity in the VP. On the other hand, the habenula-projecting globus pallidus (GPh) innervates the lateral portion of the LHb with synapses that co-release GABA and glutamate (Shabel et al., 2014). Neurons in this portion of the LHb project to the ventral tegmental area and participate in outcome evaluation during reinforcement learning (Hong and Hikosaka, 2008; Stephenson-Jones et al., 2016). Thus, there appears to be parallel LHb circuits for distinct aspects of motivational behaviors.

Previous *in vivo* recording data have shown that VP neurons encode a number of variables related to motivation such as the expected reward value (Tachibana and Hikosaka, 2012; Tian et al., 2016), state and action values (Ito and Doya, 2009; Saga et al., 2017; Tachibana and Hikosaka, 2012), as well as reward prediction error (Tian and Uchida, 2015). In line with these findings, the activity of a subset of our value coding PVNs could

be characterized as encoding reward prediction error or state value. Despite this, our data suggest that value coding PVNs represent one continuous variable with different neurons responding to motivationally relevant cues with different durations. An alternative variable has been suggested to account for the activity pattern of VP neurons, this is incentive value, or the degree to which stimuli have the ability to activate motivational states (Richard et al., 2016, 2018; Smith et al., 2009). This variable may better account for the PVN activity that we describe here, because it relates both the external stimulus value as well as the internal state of the animal (Berridge, 2012). This is important because previous recordings, as does our study, show that the activity of VP neurons depends on the internal motivational state of the animal as well as the external environment (Smith et al., 2009; Tindell et al., 2006). In light of these findings, we propose that value coding PVNs and NVNs encode incentive and aversive value, respectively.

In our recordings, the identified glutamatergic VP neurons seem to be homogeneous, only belonging to NVNs. One caveat to this finding is that, because the glutamatergic neurons in the VP are sparse, we were only able to tag a small number of these neurons. Future experiments where different methods, such as calcium imaging, are used to simultaneously record a large number of neurons may reveal functional subpopulations within the glutamatergic neurons. Furthermore, we do not know how the expectation signals in VP neurons develop during learning. The imaging or fiber photometry methods can be used to monitor VP neuronal activities throughout learning and thus to address this outstanding question. In addition, future experiments are required to monitor the changes in activity in NVNs while optogenetically manipulating PVNs, and vice versa, and determine the contribution of such changes to behavior. Finally, how the valence-specific neurons interact with the other functional populations, the type I and type III neurons (Figure 1), in the VP during behavior also awaits further study. With regard to the last two points, we found that, in all the neurons that were simultaneously recorded during the optogenetic tagging, there was no change in the firing of the non-tagged neurons when the tagged neurons were inhibited, suggesting that the distinct VP populations are unlikely to be highly connected.

The decision to approach or avoid depends on the situation in the environment and the internal state of the animal. Here, we show that two populations of VP neurons are critical for driving approach and avoidance behavior. Each of these populations is differentially regulated by both the internal state and the predicted motivational value. These results indicate that the VP is a critical area where information about the internal state and the environmental context is combined to determine the overall behavioral strategy to either approach or avoid.

STAR★METHODS

Detailed methods are provided in the online version of this paper and include the following:

- KEY RESOURCES TABLE
- LEAD CONTACT AND MATERIALS AVAILABILITY
- EXPERIMENTAL MODEL AND SUBJECT DETAILS
- METHOD DETAILS
  - Viral vectors
  - Stereotaxic surgery
  - Immunohistochemistry
  - Fluorescent *in situ* hybridization
  - Monosynaptic tracing with pseudotyped rabies virus
  - Classical conditioning task
  - Reward-and-punishment conflict task
  - Run-for-water task
  - Run-to-avoid-air-puff task
  - Real-time place preference or aversion task
  - Self-stimulation
  - *In vivo* electrophysiology
  - *In vitro* electrophysiology
- QUANTIFICATION AND STATISTICAL ANALYSIS
- DATA AND CODE AVAILABILITY

SUPPLEMENTAL INFORMATION

Supplemental Information can be found online at https://doi.org/10.1016/j.neuron.2019.12.006.

ACKNOWLEDGMENTS

We thank Dr. Thomas Mrsic-Flogel for critically reading the manuscript, Dr. Z. Josh Huang for providing mouse strains, Ga-Ram Hwang and Dylan Rebolini for technical assistance, and members of the Li laboratory for helpful discussions. This work was supported by grants from NARSAD (to M.S.-J., S.A., and B.L.), the NIH (F32MH113316 to C.B.-R. and R01MH101214, R01MH108924, R01NS104944, and 1R01DA050374 to B.L.), Human Frontier Science Program (RGP0015/2016 to B.L.), the Stanley Family Foundation (to B.L.), Simons Foundation (344904 to B.L.), the Wodecroft Foundation (to B.L.), the Cold Spring Harbor Laboratory and Northwell Health Affiliation (to B.L.), and the Feil Family Neuroscience Endowment (to B.L.).

AUTHOR CONTRIBUTIONS

M.S.-J., C.B.-R., and B.L. designed the study. M.S.-J. and C.B.-R. conducted the majority of the experiments and analyzed data. S.A. performed the patch clamp recording experiments. A.F. performed the RNAscope experiments. X.X. generated MATLAB codes for controlling behavioral devices and data analysis. C.F.-H. performed the rabies tracing experiments. M.S. and B.L. wrote the paper with input from all authors.

DECLARATION OF INTERESTS

The authors declare no competing interests.

Received: March 30, 2019
Revised: September 23, 2019
Accepted: December 4, 2019
Published: January 13, 2020

REFERENCES

Berridge, K.C. (2012). From prediction error to incentive salience: mesolimbic computation of reward motivation. Eur. J. Neurosci. *35*, 1124–1143.

Callaway, E.M., and Luo, L. (2015). Monosynaptic Circuit Tracing with Glycoprotein-Deleted Rabies Viruses. J. Neurosci. *35*, 8979–8985.

Cohen, J.Y., Haesler, S., Vong, L., Lowell, B.B., and Uchida, N. (2012). Neuron-type-specific signals for reward and punishment in the ventral tegmental area. Nature *482*, 85–88.

Cohen, J.Y., Amoroso, M.W., and Uchida, N. (2015). Serotonergic neurons signal reward and punishment on multiple timescales. eLife *4*, https://doi.org/10.7554/eLife.06346.

Courtin, J., Chaudun, F., Rozeske, R.R., Karalis, N., Gonzalez-Campo, C., Wurtz, H., Abdi, A., Baufreton, J., Bienvenu, T.C., and Herry, C. (2014). Prefrontal parvalbumin interneurons shape neuronal activity to drive fear expression. Nature *505*, 92–96.

Faget, L., Zell, V., Souter, E., McPherson, A., Ressler, R., Gutierrez-Reed, N., Yoo, J.H., Dulcis, D., and Hnasko, T.S. (2018). Opponent control of behavioral reinforcement by inhibitory and excitatory projections from the ventral pallidum. Nat. Commun. *9*, 849.

Farrar, A.M., Font, L., Pereira, M., Mingote, S., Bunce, J.G., Chrobak, J.J., and Salamone, J.D. (2008). Forebrain circuitry involved in effort-related choice: Injections of the GABAA agonist muscimol into ventral pallidum alter response allocation in food-seeking behavior. Neuroscience *152*, 321–330.

Haber, S.N., and Knutson, B. (2010). The reward circuit: linking primate anatomy and human imaging. Neuropsychopharmacology *35*, 4–26.

Hangya, B., Ranade, S.P., Lorenc, M., and Kepecs, A. (2015). Central Cholinergic Neurons Are Rapidly Recruited by Reinforcement Feedback. Cell *162*, 1155–1168.

Heimer, L., Harlan, R.E., Alheid, G.F., Garcia, M.M., and de Olmos, J. (1997). Substantia innominata: a notion which impedes clinical-anatomical correlations in neuropsychiatric disorders. Neuroscience *76*, 957–1006.

Herkenham, M., and Nauta, W.J. (1977). Afferent connections of the habenular nuclei in the rat. A horseradish peroxidase study, with a note on the fiber-of-passage problem. J. Comp. Neurol. *173*, 123–146.

Herkenham, M., and Nauta, W.J. (1979). Efferent connections of the habenular nuclei in the rat. J. Comp. Neurol. *187*, 19–47.

Hong, S., and Hikosaka, O. (2008). The globus pallidus sends reward-related signals to the lateral habenula. Neuron *60*, 720–729.

Humphries, M.D., and Prescott, T.J. (2010). The ventral basal ganglia, a selection mechanism at the crossroads of space, strategy, and reward. Prog. Neurobiol. *90*, 385–417.

Inui, T., and Shimura, T. (2017). Activation of mu-opioid receptors in the ventral pallidum decreases the negative hedonic evaluation of a conditioned aversive taste in rats. Behav. Brain Res. *320*, 391–399.

Ito, M., and Doya, K. (2009). Validation of decision-making models and analysis of decision variables in the rat basal ganglia. J. Neurosci. *29*, 9861–9874.

Knowland, D., Lilascharoen, V., Pacia, C.P., Shin, S., Wang, E.H., and Lim, B.K. (2017). Distinct Ventral Pallidal Neural Populations Mediate Separate Symptoms of Depression. Cell *170*, 284–297.

Lammel, S., Lim, B.K., Ran, C., Huang, K.W., Betley, M.J., Tye, K.M., Deisseroth, K., and Malenka, R.C. (2012). Input-specific control of reward and aversion in the ventral tegmental area. Nature *491*, 212–217.

Lecca, S., Meye, F.J., Trusel, M., Tchenio, A., Harris, J., Schwarz, M.K., Burdakov, D., Georges, F., and Mameli, M. (2017). Aversive stimuli drive hypothalamus-to-habenula excitation to promote escape behavior. eLife *6*, e30697.

Li, L., Tasic, B., Micheva, K.D., Ivanov, V.M., Spletter, M.L., Smith, S.J., and Luo, L. (2010). Visualizing the distribution of synapses from individual neurons in the mouse brain. PLoS ONE *5*, e11503.

Miyamichi, K., Amat, F., Moussavi, F., Wang, C., Wickersham, I., Wall, N.R., Taniguchi, H., Tasic, B., Huang, Z.J., and He, Z. (2011). Cortical representations of olfactory input by trans-synaptic tracing. Nature *472*, 191–196.

Mogenson, G.J., Jones, D.L., and Yim, C.Y. (1980). From motivation to action: functional interface between the limbic system and the motor system. Prog. Neurobiol. *14*, 69–97.

Pan, W.X., Schmidt, R., Wickens, J.R., and Hyland, B.I. (2005). Dopamine cells respond to predicted events during classical conditioning: evidence for eligibility traces in the reward-learning network. J. Neurosci. *25*, 6235–6242.

Panagis, G., Miliaressis, E., Anagnostakis, Y., and Spyraki, C. (1995). Ventral pallidum self-stimulation: a moveable electrode mapping study. Behav. Brain Res. *68*, 165–172.

Panagis, G., Nomikos, G.G., Miliaressis, E., Chergui, K., Kastellakis, A., Svensson, T.H., and Spyraki, C. (1997). Ventral pallidum self-stimulation induces stimulus dependent increase in c-fos expression in reward-related brain regions. Neuroscience *77*, 175–186.

Penzo, M.A., Robert, V., Tucciarone, J., De Bundel, D., Wang, M., Van Aelst, L., Darvas, M., Parada, L.F., Palmiter, R.D., He, M., et al. (2015). The paraventricular thalamus controls a central amygdala fear circuit. Nature *519*, 455–459.

Quina, L.A., Tempest, L., Ng, L., Harris, J.A., Ferguson, S., Jhou, T.C., and Turner, E.E. (2015). Efferent pathways of the mouse lateral habenula. J. Comp. Neurol. *523*, 32–60.

Richard, J.M., Ambroggi, F., Janak, P.H., and Fields, H.L. (2016). Ventral Pallidum Neurons Encode Incentive Value and Promote Cue-Elicited Instrumental Actions. Neuron *90*, 1165–1173.

Richard, J.M., Stout, N., Acs, D., and Janak, P.H. (2018). Ventral pallidal encoding of reward-seeking behavior depends on the underlying associative structure. eLife *7*, e33107.

Root, D.H., Melendez, R.I., Zaborszky, L., and Napier, T.C. (2015). The ventral pallidum: Subregion-specific functional anatomy and roles in motivated behaviors. Prog. Neurobiol. *130*, 29–70.

Saga, Y., Richard, A., Sgambato-Faure, V., Hoshi, E., Tobler, P.N., and Tremblay, L. (2017). Ventral Pallidum Encodes Contextual Information and Controls Aversive Behaviors. Cereb. Cortex *27*, 2528–2543.

Schmitzer-Torbert, N., Jackson, J., Henze, D., Harris, K., and Redish, A.D. (2005). Quantitative measures of cluster quality for use in extracellular recordings. Neuroscience *131*, 1–11.

Schultz, W., Dayan, P., and Montague, P.R. (1997). A neural substrate of prediction and reward. Science *275*, 1593–1599.

Seo, C., Guru, A., Jin, M., Ito, B., Sleezer, B.J., Ho, Y.Y., Wang, E., Boada, C., Krupa, N.A., Kullakanda, D.S., et al. (2019). Intense threat switches dorsal raphe serotonin neurons to a paradoxical operational mode. Science *363*, 538–542.

Shabel, S.J., Proulx, C.D., Piriz, J., and Malinow, R. (2014). Mood regulation. GABA/glutamate co-release controls habenula output and is modified by antidepressant treatment. Science *345*, 1494–1498.

Skoubis, P.D., and Maidment, N.T. (2003). Blockade of ventral pallidal opioid receptors induces a conditioned place aversion and attenuates acquisition of cocaine place preference in the rat. Neuroscience *119*, 241–249.

Smith, K.S., and Berridge, K.C. (2005). The ventral pallidum and hedonic reward: neurochemical maps of sucrose "liking" and food intake. J. Neurosci. *25*, 8637–8649.

Smith, K.S., Tindell, A.J., Aldridge, J.W., and Berridge, K.C. (2009). Ventral pallidum roles in reward and motivation. Behav. Brain Res. *196*, 155–167.

Stamatakis, A.M., and Stuber, G.D. (2012). Activation of lateral habenula inputs to the ventral midbrain promotes behavioral avoidance. Nat. Neurosci. *15*, 1105–1107.

Stamatakis, A.M., Jennings, J.H., Ung, R.L., Blair, G.A., Weinberg, R.J., Neve, R.L., Boyce, F., Mattis, J., Ramakrishnan, C., Deisseroth, K., and Stuber, G.D. (2013). A unique population of ventral tegmental area neurons inhibits the lateral habenula to promote reward. Neuron *80*, 1039–1053.

Stephenson-Jones, M. (2019). Pallidal circuits for aversive motivation and learning. Curr. Opin. Behav. Sci. *26*, 82–89.

Stephenson-Jones, M., Yu, K., Ahrens, S., Tucciarone, J.M., van Huijstee, A.N., Mejia, L.A., Penzo, M.A., Tai, L.H., Wilbrecht, L., and Li, B. (2016). A basal ganglia circuit for evaluating action outcomes. Nature *539*, 289–293.

Stopper, C.M., and Floresco, S.B. (2014). What's better for me? Fundamental role for lateral habenula in promoting subjective decision biases. Nat. Neurosci. *17*, 33–35.

Stratford, T.R., Kelley, A.E., and Simansky, K.J. (1999). Blockade of GABAA receptors in the medial ventral pallidum elicits feeding in satiated rats. Brain Res. *825*, 199–203.

Tachibana, Y., and Hikosaka, O. (2012). The primate ventral pallidum encodes expected reward value and regulates motor action. Neuron *76*, 826–837.

Tian, J., and Uchida, N. (2015). Habenula Lesions Reveal that Multiple Mechanisms Underlie Dopamine Prediction Errors. Neuron *87*, 1304–1316.

Tian, J., Huang, R., Cohen, J.Y., Osakada, F., Kobak, D., Machens, C.K., Callaway, E.M., Uchida, N., and Watabe-Uchida, M. (2016). Distributed and Mixed Information in Monosynaptic Inputs to Dopamine Neurons. Neuron *91*, 1374–1389.

Tindell, A.J., Smith, K.S., Peciña, S., Berridge, K.C., and Aldridge, J.W. (2006). Ventral pallidum firing codes hedonic reward: when a bad taste turns good. J. Neurophysiol. *96*, 2399–2409.

Tooley, J., Marconi, L., Alipio, J.B., Matikainen-Ankney, B., Georgiou, P., Kravitz, A.V., and Creed, M.C. (2018). Glutamatergic Ventral Pallidal Neurons Modulate Activity of the Habenula-Tegmental Circuitry and Constrain Reward Seeking. Biol. Psychiatry *83*, 1012–1023.

Wulff, A.B., Tooley, J., Marconi, L.J., and Creed, M.C. (2018). Ventral pallidal modulation of aversion processing. Brain Res. *1713*, 62–69.

Ydenberg, R.C., and Dill, L.M. (1986). The economics of fleeing from predators. Adv. Study Behav. *16*, 229–249.

STAR★METHODS

KEY RESOURCES TABLE

REAGENT or RESOURCE	SOURCE	IDENTIFIER
Antibodies		
Chicken anti-GFP	Aves Labs	Cat# GFP1020; RRID: AB_10000240
Rabbit anti-RFP	Rockland	Cat# 600-401-379; RRID: AB_2209751
Rabbit anti-Substance P	ImmunoStar	Cat# 20064; RRID: AB_572266
Bacterial and Virus Strains		
AAV9-Ef1a-DIO-hChR2(H134R)-eYFP	University of North Carolina vector core facility (Chapel Hill, North Carolina, USA)	N/A
AAV9-CAG-FLEX-ArchT-GFP	University of North Carolina vector core facility (Chapel Hill, North Carolina, USA)	N/A
AAV9-Ef1a-DIO-eYFP	University of Pennsylvania vector core (Pennsylvania, USA)	N/A
AAV-TRE-hGFP-TVA-G	University of North Carolina vector core facility (Chapel Hill, North Carolina, USA)	N/A
rabies-EnvA-SAD-ΔG-mCherry	Viral Vector Core Facility at Salk Institute	N/A
Chemicals, Peptides, and Recombinant Proteins		
Alexa Fluor 555 Conjugate Cholera Toxin Subunit B	Thermo Fisher	Cat# C22843
Critical Commercial Assays		
RNAscope Probe against *Gad2*	ACDBio	Cat# 439371
RNAscope Probe against *Slc17a6* (Vglut2)	ACDBio	Cat# 319171-C3
Experimental Models: Organisms/Strains		
Mouse: *Vglut2-Cre* (*Slc17a6*$^{tm2(cre)Lowl}$/*J*)	The Jackson Laboratory	JAX: 016963; RRID: IMSR_JAX:016963
Mouse: *GAD2-IRES-Cre* (*Gad2*$^{tm2(cre)Zjh}$/*J*,)	The Jackson Laboratory	JAX: 010802; RRID: IMSR_JAX:010802
Mouse: *Ai40D* (*Gt(ROSA)*$_{26Sor}$$^{tm40.1(CAG-aop3/GFP)Hze/J}$)	The Jackson Laboratory	JAX: 021188; RRID: IMSR_JAX:021188
Mouse: *Rosa26-stop*^{flox}*-tTA*	The Jackson Laboratory	JAX: 012266; RRID: IMSR_JAX:012266

LEAD CONTACT AND MATERIALS AVAILABILITY

Further information and requests for resources and reagents should be directed to and will be fulfilled by the Lead Contact Bo Li (bli@cshl.edu). This study did not generate new unique reagents.

EXPERIMENTAL MODEL AND SUBJECT DETAILS

All procedures were approved by the Institutional Animal Care and Use Committee of Cold Spring Harbor Laboratory (CSHL) and conducted in accordance to the United States' National Institutes of Health guidelines. Mice were housed under a 12 h light-dark cycle (8 a.m. to 8 p.m. light). All behavioral experiments were performed during the light cycle. All mice had free access to food, but water was restricted for mice used in certain behavioral experiments. Free water was provided on days with no experimental sessions. Male and female mice 2-4 months of age were used in all experiments. No differences were observed in the behavior of male or female mice during the behavioral tasks (see Figure S6 and Table S1). All animals were randomly allocated to the different experimental conditions used in this study. The *Vglut2-Cre* (*Slc17a6*$^{tm2(cre)Lowl}$/*J*, stock #016963 from Jackson Laboratory, Bar Harbor, Maine, USA), *GAD2-IRES-Cre* (from Dr. Z. Josh Huang, CSHL, available from Jackson Laboratory, *Gad2*$^{tm2(cre)Zjh}$/*J*, stock # 010802), *Ai40D* (*Gt(ROSA)*$_{26Sor}$$^{tm40.1(CAG-aop3/GFP)Hze/J}$), stock #021188 from Jackson Laboratory), *Rosa26-stop*^{flox}*-tTA* (stock #012266 from Jackson Laboratory) (Li et al., 2010; Penzo et al., 2015) mouse strains have all been previously characterized. All mice were bred onto a C57BL/6J background.

METHOD DETAILS

Viral vectors

All adeno-associated viruses (AAV) were produced by the University of North Carolina vector core facility (Chapel Hill, North Carolina, USA) or the University of Pennsylvania vector core (Pennsylvania, USA) and have previously been described: AAV9-Ef1a-DIO-hChR2(H134R)-eYFP, AAV9-CAG-FLEX-ArchT-GFP, AAV9-Ef1a-DIO-eYFP and AAV-TRE-hGFP-TVA-G. The EnvA-pseudotyped, protein-G-deleted rabies-EnvA-SAD-ΔG-mCherry virus (Miyamichi et al., 2011) was produced by the Viral Vector Core Facility at Salk Institute. All viral vectors were aliquoted and stored at –80°C until use.

Stereotaxic surgery

Mice were anesthetized with isoflurane inhalant gas (3%) in an induction chamber and positioned in a stereotaxic frame (myNeuroLab, Leica Microsystems Inc., Buffalo Grove, Illinois, USA). Isoflurane (1.5%) was be delivered through a facemask for anesthesia maintenance. Lidocaine (20 μl) was injected subcutaneously into the head and neck area as a local anesthetic. For *in vivo* recordings, mice were implanted with a head-bar and a microdrive containing the recording electrodes and an optical fiber. Viral injections were performed using previously described procedures (Penzo et al., 2015) at the following stereotaxic coordinates: VP, 0.75 – 0.30 mm from bregma, 1.00 mm lateral from midline, and 5.10 mm ventral from cortical surface; LHb, –1.82 mm from bregma, 0.40 mm lateral from midline, and 2.46 mm ventral from cortical surface; and DR, −4.24 mm from bregma, 0 mm lateral from midline, and 3.00 mm ventral from cortical surface. During the surgical procedure, mice were kept on a heating pad and were brought back to their home-cage for post-surgery recovery and monitoring. Postoperative care included intraperitoneal injection with 0.3-0.5 mL of Lactated Ringer's solution and Metacam (1-2 mg kg^{-1} meloxicam; Boehringer Ingelheim Vetmedica, Inc., St. Joseph, Missouri, USA) for analgesia and anti-inflammatory purposes. All AAVs were injected at a total volume of approximately 0.2 μl, and were allowed at least 4 weeks for maximal expression. For retrograde tracing of projection cells in the VP, CTB-555 (0.2 μl, 0.5% in phosphate-buffered saline (PBS); Invitrogen, Thermo Fisher Scientific, Waltham, Massachusetts, USA) was injected into the LHb or DR and allowed 5 days for sufficient retrograde transport.

Immunohistochemistry

Immunohistochemistry experiments were performed following standard procedures. Briefly, mice were anesthetized with Euthasol (0.4 ml; Virbac, Fort Worth, Texas, USA) and transcardially perfused with 40 mL of PBS, followed by 40 mL of 4% paraformaldehyde in PBS. Coronal sections (50 μm) were cut using a freezing microtome (Leica SM 2010R, Leica). Sections were first washed in PBS (3 × 5 min), incubated in PBST (0.3% Triton X-100 in PBS) for 30 min at room temperature (RT) and then washed with PBS (3 × 5 min). Next, sections were blocked in 5% normal goat serum in PBST for 30 min at RT and then incubated with primary antibodies overnight at 4°C. Sections were washed with PBS (5 × 15 min) and incubated with fluorescent secondary antibodies at RT for 1 h. After washing with PBS (5 × 15 min), sections were mounted onto slides with Fluoromount-G (eBioscience, San Diego, California, USA). Images were taken using a LSM 710 laser-scanning confocal microscope (Carl Zeiss, Oberkochen, Germany). The primary antibodies used were: chicken anti-GFP (1:1000, Aves Labs, catalog number GFP1020, lot number GFP697986), rabbit anti-RFP (1:1000, Rockland, catalog number 600-401-379, lot number 34135), and rabbit anti-Substance P (SP) (1:1000, ImmunoStar, catalog number 20064, lot number 1531001). Primary antibodies were incubated with appropriate fluorophore-conjugated secondary antibodies (1:1000, Life Technologies, Carlsbad, California, USA) depending on the desired fluorescence color.

Fluorescent *in situ* hybridization

Single molecule fluorescent *in situ* hybridization (ACDBio, RNAscope) was used to detect expression of *Gad2* and *Slc17a6* in LHb-projecting VP neurons. Alexa Fluor 555 Conjugate Cholera Toxin Subunit B (CTB555, Thermo Fisher Cat. No. C22843) was injected unilaterally into the LHb of wild-type adult mice. After 5 days, mice were decapitated and their brain tissue was first embedded in cryomolds (Sakura Finetek, Ref 4566) filled with M-1 Embedding Matrix (Thermo Scientific, Cat. No. 1310) then quickly fresh-frozen on dry ice. The tissue was stored at −80°C until it was sectioned. 12 μm cryostat-cut sections containing VP were collected rostro-caudally in a series of four slides and stored at −80°C, until used for hybridization. Briefly, the day of the experiment, frozen sections were post-fixed in 4% PFA in RNA-free PBS (hereafter referred to as PBS) at room temperature (RT) for 15', then washed in PBS, dehydrated using increasing concentrations of ethanol in water (50% once, 70% once, 100% twice) for 5'. Sections were then dried at RT and incubated with Protease IV for 30' at RT. Sections were washed in PBS three times for 5' at RT, then hybridized. Probes against *Gad2* (Cat. No. #439371, dilution 1:50) and *Slc17a6* (Vglut2) (Cat. No. #319171-C3, dilution 1:50) were applied to VP sections. Hybridization was carried out for 2h at 40°C. After that, sections were washed twice in PBS at RT for 2', then incubated with three consecutive rounds of amplification reagents (30', 15' and 30', respectively, at 40°C). After each amplification step, sections were washed in PBS at RT for 2', twice. Finally, fluorescence detection was carried out for 15' at 40°C. Fluorescent dyes used were Alexa 488 (for *Gad2* detection) and Atto-647 (for *Slc17a6* detection). CTB555 signal was detected in the red channel. Sections were then washed twice in PBS, incubated with DAPI (1:10000 in PBS) for 2', washed twice in PBS for 2', then mounted with coverslip using mounting medium. Images were acquired using an LSM780 confocal microscope with 20x or 40x lenses, and visualized and processed using ImageJ and Adobe Illustrator.

For quantifications of fluorescent *in situ* hybridization samples, only CTB555$^+$ cells with a clear DAPI$^+$ nucleus were counted. The percentage of CTB555$^+$ cells expressing *Gad2*, *Vglut2*, or both markers (i.e., *Gad2*$^+$*Vglut2*$^+$ cells) in total CTB555$^+$ cells were calculated based on images of the same sections from the CTB experiments. Briefly, the number of *Gad2*$^+$, *Vglut2*$^+$ and *Gad2*$^+$*Vglut2*$^+$ neurons in a region of interest (ROI) within the VP were annotated and then normalized to the area of the ROI.

Monosynaptic tracing with pseudotyped rabies virus

Retrograde tracing of monosynaptic inputs onto genetically-defined cell populations of the VP was accomplished using a previously described method (Callaway and Luo, 2015; Penzo et al., 2015). In brief, *Vglut2-Cre;Rosa26-stop*^{flox}*-tTA* or *GAD2-Cre; Rosa26-stop*^{flox}*-tTA* mice that express tTA in glutamatergic or GABAergic cells, respectively, were injected into the VP with AAV-TRE-hGFP-TVA-G (0.2–0.3 μl) that expresses the following components in a tTA-dependent manner: a fluorescent reporter histone GFP (hGFP); TVA (which is a receptor for the avian virus envelope protein EnvA); and the rabies envelope glycoprotein (G). Two weeks later, mice were injected in the same VP location with the rabies-EnvA-SAD-DG-mCherry (500 nl), a rabies virus that is pseudotyped with EnvA, lacks the envelope glycoprotein, and expresses mCherry. This method ensures that the rabies virus exclusively infects cells expressing TVA. Furthermore, complementation of the modified rabies virus with envelope glycoprotein in the TVA-expressing cells allows the generation of infectious particles, which then can *trans*-synaptically infect presynaptic neurons.

Classical conditioning task

Four *GAD2-Cre;Ai40D* and two *Vglut2-Cre;Ai40D* mice were trained on an auditory classical conditioning task. One week after surgery mice were water-deprived in their home-cage. During training, mice were head restrained using custom-made clamps and metal head-bars. Each mouse was habituated to head restraint for one day prior to training. There were five possible outcomes (unconditioned stimuli, US), each associated with a different auditory cue (conditioned stimulus, CS): a large water reward (5 μl), a small water reward (1 μl), nothing, a small air puff (100 ms) or a large air puff (500 ms). The air puff was delivered to the animal's face. Each trial began with a houselight turning on (the light stayed on for 5 s). A CS (1 s sound) was played one second after the houselight was turned on, followed by a 0.5 s delay and then a US (the outcome). For the CSs, we used 75 dB tones with 12, 10, 8, 4, 2 kHz, and 75 dB white noise.

In each session, reward and punishment trials were presented in two sequential blocks, with each cue chosen pseudorandomly. Each block contained the neutral CS. We defined satiated trials as trials where the mouse licked two or less times in the choice window.

For recording in the modified 'conflict task' (see below) the same auditory classical conditioning paradigm was used, except that one CS predicted a water reward (12 μl), another CS predicted the simultaneous delivery of both the water reward and a 100-ms air puff blowing to the face (the trials with different CSs were randomly interleaved).

Reward-and-punishment conflict task

Mice were first trained and tested in the reward-only task, and subsequently trained and tested in the reward-and-punishment conflict task (or 'conflict task'). In each trial of the reward-only task, one of five distinct auditory cues (CS; 1 s duration, presented pseudorandomly) was presented, followed by a 500-ms delay and then an outcome (US). Each CS uniquely predicted one of five sizes of water reward: 3, 5, 7, 10 or 12 μl. Water delivery was contingent on mice licking the waterspout during a 1 s choice window, which spanned the last 500 ms of CS and the 500-ms delay after CS ended. Failure of licking during the choice window led to omission of water reward. Mice were trained with one session per day (250 trials per session; inter-trial-interval, 8 s). In the optogenetic testing day, animals were subjected to 250 trials, wherein laser stimulation occurred in 20% of randomly interleaved trials (laser stimulation started from CS onset and lasted until the time of water delivery). Next, mice were trained in the 'conflict task', which was similar to the reward-only task except that licking the waterspout during the choice window triggered delivery of both the water reward and a 100-ms air puff blowing to the face.

For the reward-only part of the 'conflict task', mice were trained for 4-8 weeks until they exhibited an escalated choosing of trials during the choice window proportional to increasing reward for two days in a row, and then were tested. For the conflict part of this task, we trained mice for 1-2 weeks in the conflict situation following training in the reward-only situation. Mice were trained until they showed a 60% or less probability in choosing the biggest reward (12 ul) under the conflict situation for two days in a row before testing.

Run-for-water task

Mice were water deprived for a day prior to training in the run-for-water (RFW) task. After being habituated to the head-fixation apparatus and the running wheel, mice were presented with a CS (12-kHz, 1 s tone) that predicted the conditional availability of water (10 μl) in a spout close to the mouth. Only if the mice reached a running velocity of 10 cm/s in a response window spanning from tone onset to 500 ms after the tone ended. Failure to reach the velocity threshold during the response window resulted in water omission. Animals were trained in one session per day for 4-8 weeks (100 trials per session; average inter-trial-interval, 30 s), until they exhibited a reliable running response to the tone (2 z-scores above baseline running during any period within the CS) for two consecutive days before optogenetic testing.

For the optogenetic testing, animals received 100 trials, where 20 randomly interleaved trials included laser delivery that covered the period from CS onset to the onset of water delivery. For all optogenetic manipulations, the laser parameter used were: pulse duration, 5 ms (for ChR2) or constant light (for ArchT); frequency, 30 Hz (for ChR2) or constant light (for ArchT); train duration, 1.5 s; laser intensity, 10 mW (measured at the tip of optic fibers). Throughout the training and testing, animals were ensured to receive a total of 1 mL of water every day.

Run-to-avoid-air-puff task

Mice were habituated to the head-fixation apparatus and the running wheel prior to running-to-avoid-air-puff task (RTAA) training. Mice were then presented with auditory tones (white noise, 1 s) that predicted delivery of an air puff to the face (400 ms) if the animal did not reach a running speed of 10 cm/s at some point from tone onset to 500 ms after tone offset. Failure to reach the speed threshold resulted in punishment delivery. The intertrial interval was 30 s on average. Animals were trained every day for one session of 100 trials. Animals were trained from 4-8 weeks until they exhibited a reliable running response to the tone (2 z-scores above baseline running) before optogenetic testing. For the optogenetic testing day, animals received 100 trials, where 20 randomly interleaved trials included laser delivery that covered from tone onset to the air puff delivery time.

Real-time place preference or aversion task

Freely moving mice were initially habituated to a two-sided chamber, and were subsequently subjected to a 10-min session in which laser stimulation (laser power, 10 mW (measured at fiber tip); laser frequency, 40 Hz for ChR2 experiments or the laser was constantly on for ArchT experiments) was turned on once mice entered the left side of the chamber. This was followed by another 10-min session in which laser simulation was turned on once mice entered the right side of the chamber. We recorded the percentage of time the mice spent on either side of the chamber during baseline and during the laser stimulation.

Self-stimulation

Freely moving mice were placed in a chamber equipped with two nose-poke ports. Nose-poking to one of the ports (the active port) triggered laser delivery (pulse duration, 5 ms, train duration, 2 s, intensity, 10 mW (measured at fiber tip), frequency, 40 Hz), while nose-poking to the other port (the inactive port) did not trigger laser delivery. Mice were allowed to freely poke the two ports and were tested in a single 1-hr session.

In vivo electrophysiology

Custom-built screw-driven microdrives with 4 implantable tetrodes and a 50 μm fiber-optic were used to record simultaneously from multiple neurons. Each tetrode was glued to the fiber-optic with epoxy, such that the end of each tetrode was 200-400 μm from the end of the fiber-optic. Neural recordings and time stamps for behavioral variables were acquired with a Tucker-Davis Technologies RZ recording system (with a 32 channel preamp PZ2-32 and a RZ5D Bioamp processor; Alachua, Florida, USA).

Broadband signals from each wire were filtered between 0.2 and 8,500 Hz and recorded continuously at 25 kHz. To extract the timing of spikes, signals were band-pass-filtered between 300-5,000 Hz. Data analyses were carried out using software in MATLAB (The Mathworks, Inc., Natick, Massachusetts, USA). Spike waveforms were manually sorted offline based on amplitude and waveform energy features using MClust-3.5 (from Dr. A. David Redish, University of Minnesota, Minneapolis, Minnesota, USA). Individual neurons were only included in the dataset if they were well isolated based on their isolation distance (> 20) and L-ratio (< 0.1) (Schmitzer-Torbert et al., 2005). Prior to implantation, tetrodes were dipped in DiI to aid the post hoc visualization of the recording locations.

In order to convert raster plots of firing rate into continuous spike density functions, spike times were first binned into 1 ms time windows and then convolved with a Gaussian kernel ($\sigma = 15$ ms). To determine the response to the CS or US presentation, the average firing rates were calculated using a 300 ms window defined as 180-480 ms following the stimulus. These time windows were chosen to cover the time of the peak neuronal response. Average baseline firing was calculated using a 300 ms window immediately preceding the delivery of the CS.

To identify putative GABAergic or glutamatergic VP neurons, we used ArchT-mediated optic tagging (Courtin et al., 2014), whereby 200 ms light pulses ($\lambda = 532$ nm; OEM Laser Systems Inc., Bluffdale, Utah, USA) were delivered every 5 s for 100 trials following each behavioral recording session. In early sessions we also used 500 ms ($n = 3$) or 1 s ($n = 1$) light pulses, which tagged VP neurons in a similar way to that of the 200 ms light pulses. Units that showed rapid suppression (with latencies < 10 ms) in response to the laser stimulation and had neural activity suppressed to below 0.5Hz during laser stimulation were considered to be optogenetically tagged.

In addition to their response to light, putative VP neurons were identified based on their firing pattern through a previously described unsupervised clustering approach (Cohen et al., 2012). Briefly, the first three principal components (PCs) of the Z scored firing rates of all neurons in the reward and punishment blocks were calculated using principal component analysis (PCA), with the singular value decomposition algorithm. Hierarchical clustering of the first three PCs was then performed using a Euclidean distance metric and a complete agglomeration method.

Cross-correlations between spike waveforms across sessions were used to determine whether the same unit was recorded over multiple sessions. The cross-correlations were calculated after aligning the negative peak of each waveform, averaging separately, and aligning the peaks of the averages. A conservative session-to-session cross-correlation coefficient of > 0.95 was used to

positively classify two sets of waveforms as belonging to the same unit. The correlation was calculated using the full duration of the spike in a window 10 ms prior to and 40 ms after the peak negative response.

CS–US indices were calculated as (CS - US)/(CS + US), where CS is the difference between the peak firing rate (maximum value of the PSTH) in the 500 ms after CS onset and the baseline firing rate, and US is the difference between the peak firing rate in the 500 ms after US onset and the baseline firing rate. The baseline firing rate was calculated as the mean of the PSTH in the 0.5 s before CS onset.

To calculate receiver-operating characteristic (ROC) curves, the distributions of firing rates were compared between 1 s of activity prior to the CS presentation (baseline activity) and 1 s of activity after the CS presentation, or between the distributions of firing rates following two different cues.

In vitro electrophysiology

Patch clamp recording was performed as previously described (Penzo et al., 2015). Briefly, mice were anesthetized with isoflurane before they were decapitated; their brains were then dissected out and placed in ice chilled dissection buffer (110 mM choline chloride, 25 mM $NaHCO_3$, 1.25 mM NaH_2PO_4, 2.5 mM KCl, 0.5 mM $CaCl_2$, 7.0 mM $MgCl_2$, 25.0 mM glucose, 11.6 mM ascorbic acid and 3.1 mM pyruvic acid, gassed with 95% O_2 and 5% CO_2). An HM650 Vibrating-blade Microtome (Thermo Fisher Scientific) was then used to cut 300 μm thick coronal sections that contained the LHb. These slices were subsequently transferred to a storage chamber that contained oxygenated artificial cerebrospinal fluid (ACSF) (118 mM NaCl, 2.5 mM KCl, 26.2 mM $NaHCO_3$, 1 mM NaH_2PO_4, 20 mM glucose, 2 mM $MgCl_2$ and 2 mM $CaCl_2$, at 34°C, pH 7.4, gassed with 95% O_2 and 5% CO_2). Following 40 min of recovery time, slices were transferred to RT (20-24°C), where they were continuously bathed in the ACSF.

Whole-cell patch clamp recording from LHb neurons was obtained with Multiclamp 700B amplifiers and pCLAMP 10 software (Molecular Devices, Sunnyvale, California, USA), and was visually guided using an Olympus BX51 microscope equipped with both transmitted and epifluorescence light sources (Olympus Corporation, Shinjuku, Tokyo, Japan). DR-projecting LHb neurons retrogradely labeled with CTB555 (red fluorescent) were identified and patched. The external solution was ACSF. The internal solution contained 115 mM caesium methanesulphonate, 20 mM CsCl, 10 mM HEPES, 2.5 mM $MgCl_2$, 4 mM Na_2ATP, 0.4 mM Na_3GTP, 10 mM sodium phosphocreatine and 0.6 mM EGTA (pH 7.2).

As the acute slices were prepared from mice in which GABAergic or glutamatergic VP neurons were infected with AAV expressing ChR2-YFP, to evoke VP synaptic transmission onto LHb neurons, a blue light was used to stimulate ChR2-expressing axons originating from the VP. The light source was a single-wavelength LED system (λ = 470 nm; https://www.coolled.com/) connected to the epifluorescence port of the Olympus BX51 microscope. A light pulse of 1 ms, triggered by a TTL signal from the Clampex software, was delivered every 10 s to drive synaptic responses. Inhibitory or excitatory postsynaptic currents (IPSCs or EPSCs, respectively) were low-pass filtered at 1 KHz and recorded. IPSCs were recorded at a holding potential of 0 mV, with APV (100 μM) and CNQX (5 μM) added to the ACSF. EPSCs were recorded at holding potentials of –70 mV (for AMPA-receptor-mediated responses) and +40 mV (for NMDA-receptor-mediated responses), with picrotoxin (100 μM) added to the ACSF. Synaptic responses were analyzed using pCLAMP 10 software.

QUANTIFICATION AND STATISTICAL ANALYSIS

To determine whether parametric tests could be used, the Shapiro-Wilk Test was performed on all data as a test for normality. The statistical test used for each comparison is indicated when used. The sample sizes used in this study were based on estimations by a power analysis. Behavioral tests and electrophysiological data acquisition were performed by investigators with knowledge of the identities of experimental groups. All these experiments were controlled by computer systems, with data collected and analyzed in an automated and unbiased way. No data points were excluded.

DATA AND CODE AVAILABILITY

This study did not generate datasets/code.